Journal of Thermal Analysis and Calorimetry
https://doi.org/10.1007/s10973-024-13482-0

Synthesis, thermal, and mechanical characterisation of metakaolin-based geopolymers coloured with grape marc extract

Chiara Pelosi[1] · **Elena Pulidori**[1] · **Antonio D'Angelo**[2] · **Maria Rosaria Tiné**[1] · **Michelina Catauro**[2]

Received: 27 February 2024 / Accepted: 17 July 2024

Abstract

Over the years, several materials have been used for restoration purposes, with different types of dyes and colour hues. Recently, some researchers have proposed geopolymers (GPs) or amorphous aluminosilicate polymers for these purposes. In this work, an alcohol-based grape marc extract (GME, obtained via dark maceration assisted with ultrasound) was used as a natural dyeing agent for metakaolin-based GPs. The geopolymerisation occurrence was assessed by Fourier-transform infrared (FT-IR) spectroscopy and X-ray diffraction analysis, while the colour of the resulting material was determined through the colorimetric analysis in the *L*a*b** colour space. Additionally, the thermal stability of GME and GPs was investigated by thermogravimetry coupled with FT-IR spectroscopy. The microstructure, the reticulation stability, and the antimicrobial activity of GPs were examined through the scanning electron microscopy, the pH and ionic conductivity measurements, integrity, and mass loss tests. Overall, a coloured geopolymer with suitable thermal, antimicrobial, and mechanical properties was obtained, justifying its potential use in restoration or, more generally, in the construction field.

Graphical abstract

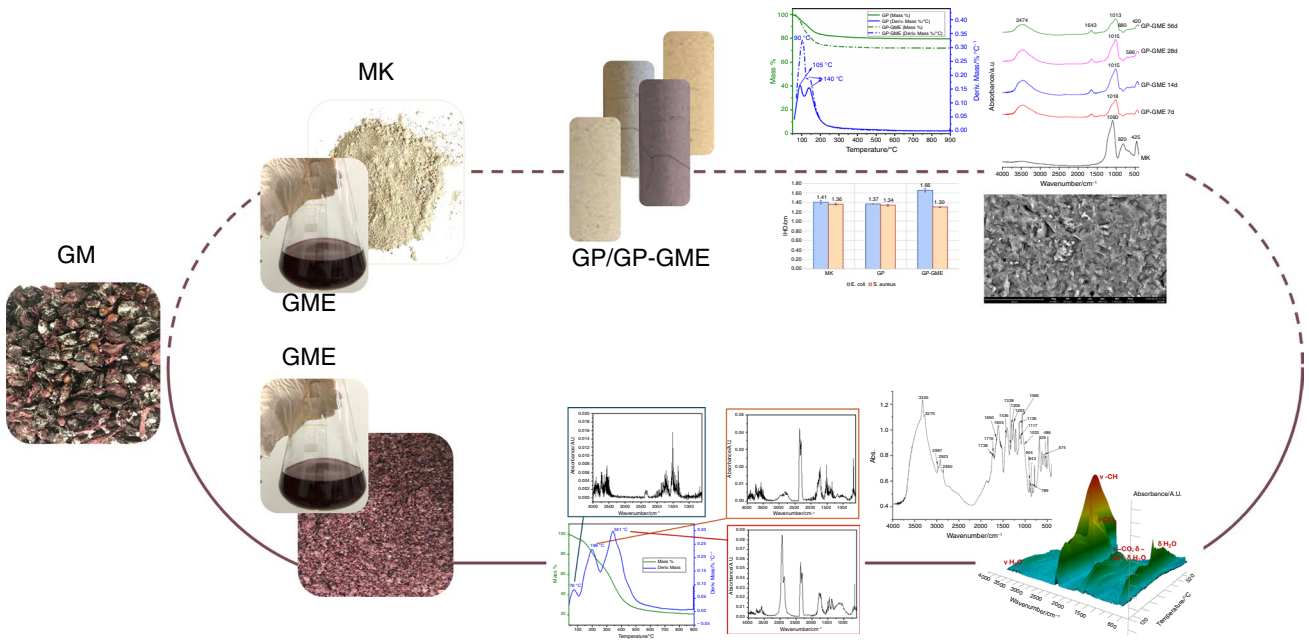

Keywords Coloured geopolymer · CIELab measurement · Antimicrobial assessment · Thermal stability · Grape marc extract

Extended author information available on the last page of the article

Published online: 24 August 2024

Introduction

Over the past decades, the importance of by-products and waste valorisation has become of great interest because of the possibility of recovering many active compounds with added value. Indeed, from the harvesting of agricultural raw materials to the development of food products, there is a considerable production of both waste and by-products that, from a Circular Economy and Sustainability perspective, represent huge sources to extract bioactive molecules (antioxidants, antimicrobials, anti-inflammatories), as well as natural dyes (e.g. carotenoids, chlorophylls, and anthocyanins) [1–4].

Italy is one of the countries with a strong agricultural tradition, and the wine sector is one of the most important productions. According to ISTAT data, wine production was 54.0 million hectolitres in 2022 [5]. Moreover, it has been estimated that the wine industry produces overall about 5 tonnes of waste per hectare of land that must be disposed of [6].

In the wine-making process, many by-products, such as stems, seeds, and grape marc (GM), can be valorised to produce value-added bioactive compounds. GM is partly sent to distilleries to make grappa and partly used as fertiliser to produce wine in subsequent vintages. Moreover, the presence of phenols, polyphenols, and flavonoids imparts to both grape skin and GM their distinctive violet colour hues. For this reason, the grapes and their derivates could be an excellent source of natural colourants, with a suitable application in the colouration of geopolymers (GPs) useful for the restoration of mosaics and indoor design objects. GPs (or inorganic amorphous aluminosilicate-based materials) are "ceramic-like" materials also known to be the main competitor of Portland Cement [7]. One of their main features is the possibility to tailor the molar ratio between SiO_2 and Al_2O_3, which allows to obtain materials for different applications [8].

Recently, the possibility of entrapping an organic dye into the GP matrix, giving colour to the material, was proposed. This approach is still novel and not fully explored, because the dye needs to be added during the geopolymerisation reaction, thus the conditions need to be carefully optimised. Just a few cases of GPs coloured with the pigment Maya blue [9] or the synthetic acridine orange [10] bromothymol blue, cresol red, phenolphthalein, and methyl orange [11] have been reported to date.

The main objective of this research is to study the feasibility of entrapping a natural dye extracted from GM in a metakaolin-based geopolymer, and the evaluation of its properties in view of future applications. Among the others, the study of the thermal properties of materials assumes great importance in assessing their applicability. For example, the determination of thermal stability, the mechanism of thermal degradation, and the assessment of the emission of toxic compounds are important information needed for the characterisation of composites [12, 13], biomasses [14, 15], polymers [16, 17], new reaction media [18], construction materials [19] (in particular geopolymers [14, 20–22]), etc., on a laboratory and an industrial scale.

More in detail, GM underwent acid–alcoholic maceration (in the dark to prevent dye decomposition), assisted by ultrasound. The extract was directly used to colour the fresh geopolymer paste before being poured into the moulds. FT-IR, XRD, and SEM analyses proved that the geopolymerisation reactions occurred properly even in the presence of the natural dye, with no changes in its microstructure, producing a coloured material. The main properties of the latter were subsequently studied by a combined approach of thermal analysis techniques, mechanical properties, stability (through pH, ionic conductivity measurements, mass loss, and integrity tests), and antimicrobial tests. The totality of the results obtained makes this coloured material attractive for future applications.

Experimental section

Materials

GM was collected in Taurasi (41° 00′ 41.3″ N 14°57′ 56.7″ E, 371 m a.s.l.), Avellino, Italy. Ethanol (EtOH 99, 9%, Sigma-Aldrich) and formic acid (96%, Sigma-Aldrich) have been used for the dye extraction. Commercial Metakaolin (MK), purchased from IMCD Deutschland GmbH & Co. (Köln, Germany) (d50 = 3.6 µm, surface area via B.E.T. method 12 $m^2\ g^{-1}$), was used as a geopolymer precursor. This MK contains 53% of SiO_2, 40.5% of Al_2O_3, and 5% of TiO_2 (mass %), and it possesses an amorphous X-ray diffraction spectrum with main crystalline phases related to the quartz and titania [10]. A mixture of sodium hydroxide (Sigma-Aldrich, Darmstadt, Germany) and sodium silicate (purchased from Prochin Italia Prodotti Chimici Industriali Srl, Marcianise, Italy), whose composition (mass %) is 27.1% of SiO_2, 8.85% of Na_2O, and 64.05% of H_2O, was used for the alkali activation.

GM extraction method

The dye extraction process was carried out with an ultrasound-assisted maceration (UAM, Branson UltrasonicsTM BransonicTM M3800-E, Danbury, USA) in the dark following the slightly modified protocol reported in Piccolella et al. 2019 [2]. Briefly, the grape marc, stored at − 20 °C, was removed from the freezer and finely ground by using

a rotary knife homogeniser (Knife Mill PULVERISETTE 11, Buch & Holm, Herlev, Denmark). One hundred grams of the organic matrix underwent a dark maceration process with a solid–liquid ratio of 1/5 m/v, using a solution of 450 mL of EtOH and 50 mL of formic acid. After 24 h of maceration, the sample was subjected to an ultrasonic cycle for 30 min and then filtered under vacuum with 0.45 µm Whatman paper to remove the non-soluble lignin–cellulosic fraction. The solid residue, i.e., the exhausted matrix, was re-extracted using the same process described above. The extraction process was repeated for a third time on the exhausted matrix obtained from the second extraction process, following the scheme summarised in Figure S1. All the fractions were collected in a 2-L bottle and concentrated under nitrogen flux until the obtainment of 500 mL of a solution containing anthocyanins. No further purifications of anthocyanins were performed. The final concentrated solution, called grape marc extract (GME, pH = 2.8), was used for the geopolymer synthesis.

Extract characterisation

GME was dried using a rotary evaporator and the obtained powder was used for its characterisation. Firstly, FT-IR was performed to characterise GME powder. The spectrum was acquired in the range of 4000–400 cm^{-1} (resolution 2 cm^{-1}, 64 scans) employing the Prestige21 Shimadzu system (Shimadzu, Milan, Italy). For the analysis, 2 mg of sample powder was mixed with 198 mg of dried KBr. The spectrum was analysed with IR Solution software, whereas the plots were done with Origin Pro 9.0.

Thermogravimetric analysis (TGA) was performed with a thermobalance (TA Instrument, model Q5000IR) coupled with an FT-IR Agilent Technologies spectrophotometer (Cary 640) for evolved gas analysis (EGA). The platinum crucible was loaded with approximately 20 mg of the sample and heated from 25 to 900 °C, at a heating rate of 20 °C min^{-1} under nitrogen flow (30 mL min^{-1}). FT-IR spectra of the gases evolved during the thermal scan were acquired in a wavelength range of 4000–600 cm^{-1} every 14 s with a 4 cm^{-1} width slit. The optical bench was purged with nitrogen and a background spectrum was recorded before each analysis. Mass and temperature calibrations of thermobalance were performed using certified mass standards supplied by TA Instruments. The curves were analysed with the software TA Universal Analysis 2000 (version 4.5A) and the FT-IR spectra with ResPro Evolution (version 5.2.0). Data were plotted with Origin Pro 9.0.

Geopolymer synthesis

The comparative study of geopolymers with and without the addition of GME was carried out by keeping all the parameters constant, i.e., liquid/solid ratio, mixing sequence, curing, and hardening procedure, as reported in [10]. An AUCMA stand mixer SM-1815Z (AUCMA Co., Ltd., Qingdao, China) was used to produce the geopolymers. The synthesis sequence can be divided into two steps, the first one consists of mixing the MK powder (50.0 g) with the activating solution (79.4 g of sodium hydroxide/sodium silicate solution) at low speed for 10 min, followed by the mixing of the fresh geopolymer paste with 4 mL of GME at high speed for 10 min. The resulting sample was called GP-GME. The control GP was synthesised following the same procedure, without the addition of GME. After the mixing procedure, the fresh geopolymer pastes were put into plastic moulds and cured for 24 h at a constant temperature of 25 °C with a Binder MB6 (Binder GmbH, Tuttlingen, Germany). After that, the samples were taken out of the oven and aged for 7, 14, 28, and 56 days at room temperature.

Geopolymers' characterisation

Scanning electron microscopy (SEM) was performed with Alfatest Phenoma XL G2 (Rome, Italy) to obtain information GPs microstructure. The chemical stability of the geopolymers was investigated as suggested in the literature [23]. The samples were ground using a Retsch RM100 Mortar Grinder (Retsch GmbH, Haan, Germany) for three minutes at 90 rpm with adjustable spring pressure. The powdered materials were sieved at d < 125 µm before analysis. To measure both pH and ionic conductivity, the GP and GP-GME powders were soaked in deionised water (1/10 m/v). The ionic conductivity and pH values were collected at different times (from 0 min up to 72 h) for all aged samples. Ionic conductivity measurements were carried out with a Crison GLP31, whereas the pH measurements were performed with a Crison GLP21, both purchased by Hach Lange S.L.U., Barcelona, Spain. Three independent measurements were performed to measure the standard deviation.

Integrity tests were performed following this procedure: GP and GP-GME at different ageing times were soaked in Milli-Q water at room temperature (1/100 m/v) for 24 h. The reticulation integrity was evaluated by measuring the pH and the colour of the water, and by observing the eventual presence of fractures in the material.

The mass loss tests were carried out according to the following procedure: at first, GPs were broken into large pieces, soaked for 3 h in acetone, dried in an oven at 25 °C, weighed (M_i) and soaked in Milli-Q water (1:100 m:v) for 24 h; after that, the pieces were removed from the water, soaked for 3 h in acetone and then left in the oven at 25 °C for 3 h; finally, the pieces were weighed (M_f), and the percentage of mass loss (M_L,%) was calculated following Eq. 1 [24]:

$$M_L\% = \frac{M_i - M_f}{M_i} * 100 \quad (1)$$

Measurements were performed in triplicate and values are reported as average ± standard deviation.

The compressive strength (σ max) tests on five cubic (5 cm × 5 cm × 5 cm) specimens for each formulation were carried out by using an Instron 5567 electromechanical testing machine (maximum load 10 kN) at a constant displacement rate of 5 mm/min on GP and GP-GME samples aged at 28 days, according to European standard EN 826 [25].

The colour of the GP-GME was assessed by using a colorimeter (Colorimeter PCE-CSM 6, PCE Holding GmbH, Hamburg, Germany) in the UV–visible range of 300–800 nm. The instrument defines the colours in the CIELab space (also referred to as L*a*b* colour space defined by the International Commission on Illumination, abbreviated CIE in 1976). Measurements led to the determination of the parameter ΔE to assess the colour difference between two samples [26] (in this case the white control GP and GP-GME). ΔE value was measured following the equations reported in [11].

FT-IR spectra of the GPs were acquired at different ageing times, whereas their thermogravimetric analyses (coupled with FT-IR analysis on evolved gas) were performed after 56 days of ageing, both following the procedures reported in paragraph 2.3. Moreover, XRD power diffraction patterns of MK precursor, and GP and GP-GME samples after 56 days of ageing were collected at the Dipartimento di Scienze della Terra of the Università di Pisa, on a Bruker D2 phaser diffractometer, equipped with a Lynxeye detector, operating at 30 kV and 10 mA and using Cu Kα radiation ($\lambda = 1.54184$ Å). Diffraction data were collected over the 6°–70° 2θ range, with scan step 0.02° and a long counting time (49, 2 s per step).

Finally, the antibacterial test was performed by using the Kirby–Bauer method [27] on *S. aureus* (Gram-positive) and *E. coli* (Gram-negative) microbial strains. The whole protocol can be divided into five steps, involving the agar-based media preparation, the sample preparation and sterilisation, the bacterial strain preparation and incubation, and the measurements of inhibition halo diameters (IHD, cm) and bacterial viability (BV, %) after the incubation time. The detailed procedure can be found elsewhere in [10]. For this test, GP and GP-GME were assayed after 56 days of ageing time.

Results and discussion

GME characterisation

The GME was characterised through FT-IR spectroscopy. The obtained spectrum, reported in Fig. 1, is rich

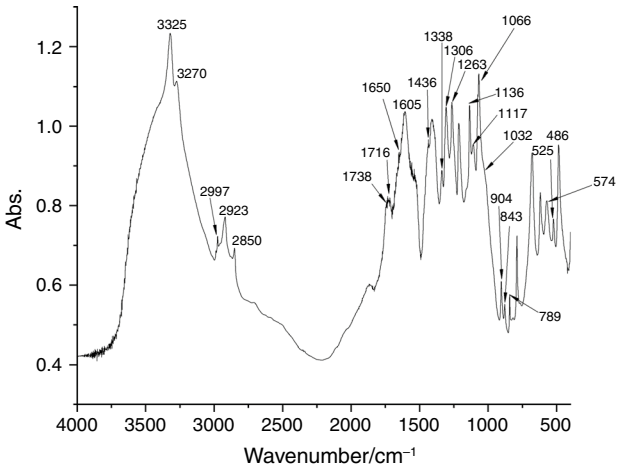

Fig. 1 FT-IR spectrum of GME

in absorption peaks, suggesting the complexity of the extract. The absorption band at 3325 cm^{-1} is related to –OH stretching [28, 29], and together with the signal at 1066 cm^{-1} (C–O– stretching), indicates the presence of polysaccharides [29]. According to Farru et al. 2022, both these signals are also related to N–H and C–N stretching of aminosugars present in the extract [30]. The O–H absorption band at 3270 cm^{-1} is related to the wagging vibration of phenolic O–H [31], whereas the signals in the range of 2997–2850 cm^{-1} are assigned to C-H vibrations [29]. The absorption bands at 1738 and 1716 cm^{-1} are assigned to C=O stretching [29, 31]. The band at 1650 cm^{-1} is assigned to H–O–H bending [28], while according to [32], the signal at 1605 cm^{-1} is assigned to the C=C–O deformation of heterocyclic C–ring of flavonoid moiety. This absorption band is also related to the CH_2 and CH_3 vibration of flavonoid rings [31]. Moreover, the C–C stretching at 1338 cm^{-1} is assigned to the aromatic ring [29, 30]. In the extract, there are also absorption bands coming from the presence of tannin compounds, such as the absorption band at 1263 cm^{-1} that is typical of flavonoid-based tannins [31], or the C–O weak stretch and C–C–OH signals at 1117 cm^{-1} and 843 cm^{-1} [32]. This latter is also related to the flavanol heterocyclic ring [32]. The absorption bands at 1136 cm^{-1} and 1032 cm^{-1} (here as a shoulder) are assigned to C–O–C and C–O–H of phenolic sugars [31]. Finally, the absorption band at 904 cm^{-1}, and 574–485 cm^{-1} are related to C–H, C–C, and C–O bending of the heterocyclic C ring [29–31].

The thermal degradation of GME under a nitrogen atmosphere was studied by TGA and TGA coupled with an FT-IR spectrometer to analyse the gases released during degradation. The thermal profile (reported in Fig. 2a) shows that the degradation occurs in four main regions of mass loss: the first region below 100 °C (5% mass loss), the second in the range 100–250 °C (25% mass loss), the

third in the range 250–500 °C (44% mass loss). An additional 7% of mass loss occurs in between 700 and 900 °C. After heating to 900 °C, 21% of the initial mass remains as a carbonaceous organic residue.

The FT-IR spectra of evolved gases helped to identify the main functional groups present in the decomposition products. The initial mass loss, below 100 °C, is primarily attributed to moisture evaporation confirmed by the presence of characteristic peaks in the spectrum (O–H stretching: 4000–3300 cm^{-1}, H–O–H bending 1700–1500 cm^{-1}). The FT-IR spectrum recorded at 196 °C reveals the presence of several functional groups: O–H stretching and H–O-H bending, indicating continuous water release and dehydroxylation reactions; CO_2 stretching and bending (at 2450–2250 and 730–580 cm^{-1}, respectively), indicating the formation of carbon dioxide during degradation; a weak doublet observed between 2000 and 2200 cm^{-1} indicating the presence of carbon monoxide. Furthermore, broad signals in the range of 3000–2600 cm^{-1}might be attributed to the stretching of C–H bonds, while the signals in the range of 1200–900 cm^{-1} could be attributed to the C–H bending and C–O stretching of volatile phenols. A further increase in temperature (see spectrum at 341 °C) caused a substantial increase in the intensity of the C-H signals, and the appearance of a peak with two maxima, at 1732 and 1716 cm^{-1}, respectively, related to the stretching of the carbonylic group [33]. Furthermore, at 375 °C (see Figure S2) the appearance of a peak with a maximum at 3015 cm^{-1} was observed, due to the evolution of gaseous CH_4 [34]. Overall, the observed peaks are consistent with findings reported in studies on grape marc pyrolysis [29, 34, 35] considering the lack of non-soluble lignin, cellulose, and hemicellulose fractions in our samples.

To elucidate the potential pathways involved in the thermal degradation of GME, the variation of the area of specific infrared bands during the degradation was evaluated. Figure 2b, c shows the temperature-resolved FT-IR analysis. The presence of signals at 4000–3300 cm^{-1} and 1700–1500 cm^{-1} in the temperature range 25–500 °C, suggests ongoing release of water molecules. This can be attributed to the loss of moisture and adsorbed water, likely occurring at lower temperatures, and to the dehydroxylation of polysaccharides and/or polyphenols involving the removal of hydroxyl groups from these biomolecules. The bands related to C–H and –(C=O) stretching vibrations suggest their thermal cracking forming volatile organic molecules. The cracking process starts at relatively low temperatures, around 200 °C, but the most significant effect occurs at around 400 °C. Another significant phenomenon is the release of CO_2, indicating the decarbonation of the previously cited components. Besides, a possible contribution to CO_2 formation may be given by the decomposition of residual carbonate minerals from grape marc present in GME extract [34]. Finally, the presence of CH_4 may be given by the decomposition of phenols at high temperatures [36].

Geopolymer stability

In order to assess the occurrence of the geopolymerisation, FT-IR analysis was performed on MK, GPs, and GP-GME samples obtained at different ageing times. In particular, the shift of the DOSPM (density of state peak maximum) relative to the MK absorption band at 1090 cm^{-1} was studied [11, 37]. Indeed, it has been demonstrated that when the geopolymerisation takes place, the band at 1090 cm^{-1}, associated with the asymmetric stretching of Si–O–T (T = Si or Al), shifts to a lower wavenumber, in this case, up to 1011 and 1013 cm^{-1} after 56 days of ageing time (see Fig. 3a and b) in the GP and GP-GME samples, respectively. This shift has been attributed to the substitution of Si^{4+} by Al^{3+} atoms in the 3D reticulation [37]. In MK and GP samples (Fig. 3a), the bands at 820 and 880 cm^{-1} were assigned to Al(IV)–OH and Al(IV)–O^- vibrations, while the signals at 3465, 1660, and 465 cm^{-1} were identified as –OH stretching and bending vibrations, originating from both water and silanol molecules [38, 39]. Besides, by observing the spectra shown in Fig. 3b for the GP-GME samples obtained at different ageing times, a shift of DOSPM towards a lower wavelength can be observed, thus suggesting that the dye extract does not have a negative influence on the geopolymerisation reactions.

The occurrence of geopolymerisation reaction was confirmed also by the comparison of the XRD diffraction pattern of MK, GP, and GP-GME (Figure S3). MK (Figure S3a) reveals a main amorphous hump between 15 and 35° (2θ) with sharp reflections due to TiO_2 crystalline phase impurities. XRD diffraction patterns of GP and GP-GME after 56 days of ageing (Figure S3b) displayed a similar amorphous hump shifted to the right, to the range 20–40° (2θ), typical for a "well-formed" geopolymers [10, 40–42], on which a sharp reflection ascribed to the TiO_2 impurities is present. Moreover, it can be observed that GP and GP-GME present the same XRD patterns, meaning that the presence of the organic extract did not change the mineralogical form of the geopolymer, and thus it did not interfere with the geopolymerisation process.

After getting evidence of the success of the geopolymerisation reaction, the thermal stability of the blank (GP) and coloured (GP-GME) geopolymer was assessed by TGA-FT-IR analyses (Fig. 4) after 56 days of ageing. The thermal profile of the geopolymer aligns with findings reported in recent studies on similar materials [43]. The primary observation is the loss of the water entrapped during the geopolymerisation process, as confirmed by the FT-IR spectra (see Figure S4a, b), which likely show characteristic peaks associated with water molecules. The dehydration process is divided into two steps (as highlighted by the presence of two maxima in

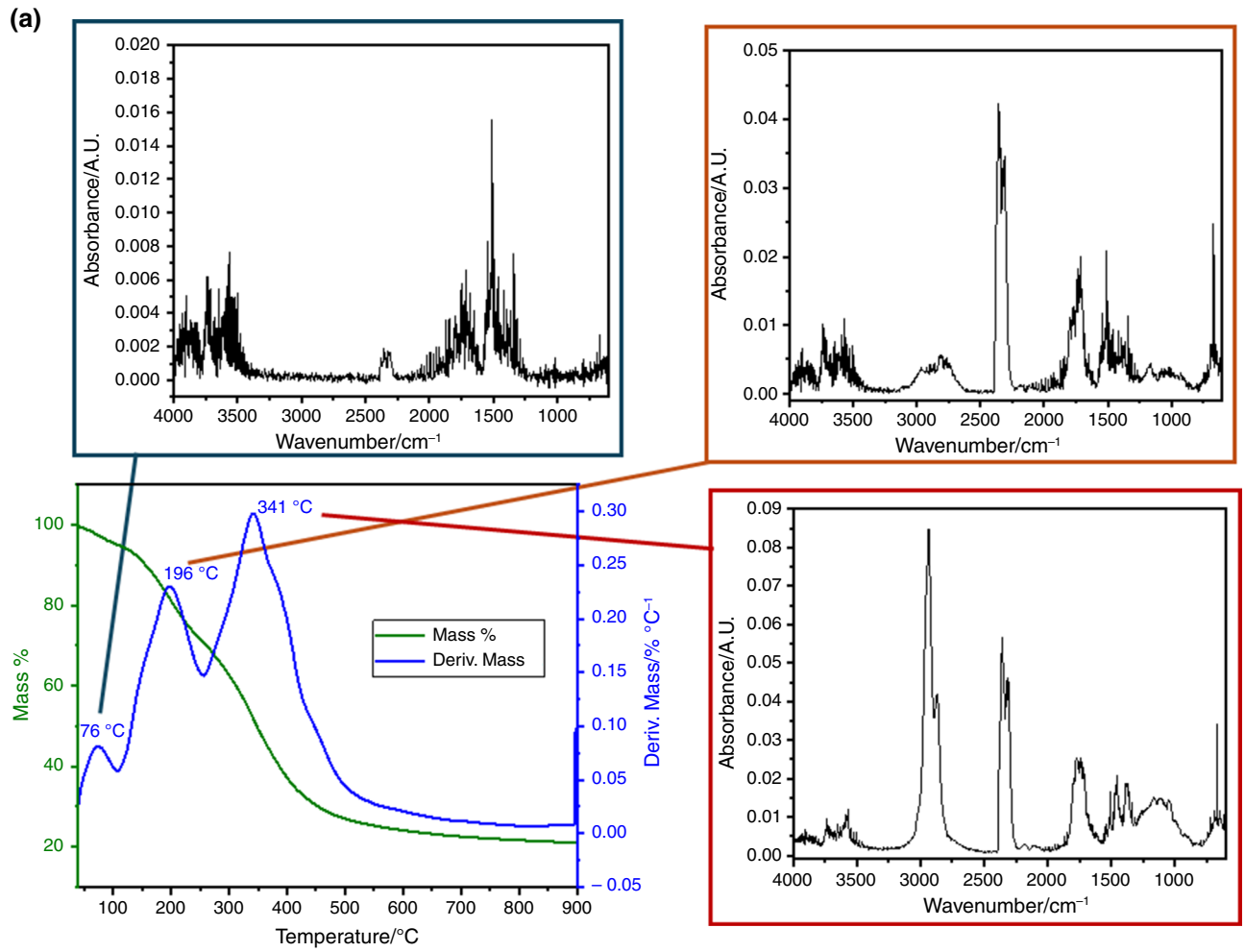

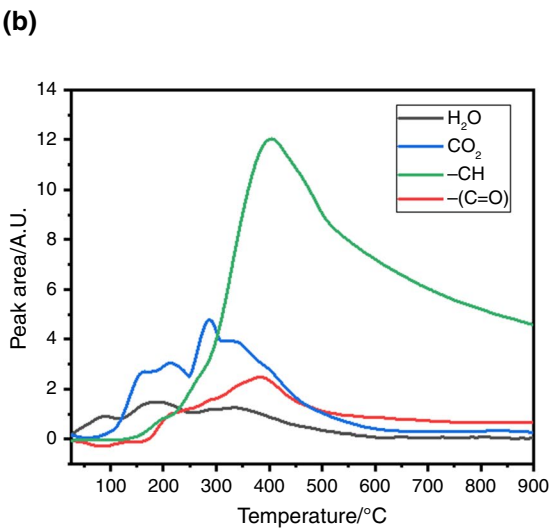

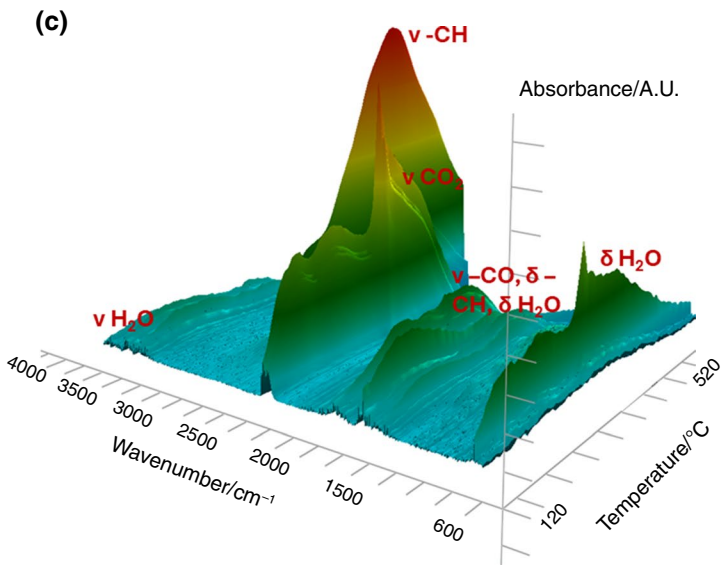

the derivative curve, reported in blue): i) below 100 °C there is the loss of water adsorbed on the external surface and ii) between 100 and 150 °C the loss of water trapped within the geopolymer's internal structure [44]. The presence of GME increases the total amount of water adsorbed by the geopolymeric matrix (from 18 to 26% mass loss). Moreover, the maximum of the first peak in the derivative curve shifts from 90 to 105 °C. This suggests that water in the GP-GME

◂**Fig. 2** **a** Thermogravimetric profile (TG, in green) and its derivative (DTG, in blue) of GME obtained by TGA, and FT-IR analyses of the gases evolved during thermal degradation. The FT-IR spectra were recorded in the range 4000–600 cm^{-1} at, respectively, 76, 196, and 341 °C (from left to right); **b** Evolution profiles of the main functional groups detected in GME thermal degradation, obtained by plotting the variation in the area of the corresponding signals over temperature scan (stretching at 4000–3300 cm^{-1} for H_2O; stretching at 2450–2250 cm^{-1} for H_2O; stretching at 3000–2600 cm^{-1} for the –CH substituents, stretching at 1800–1600 cm^{-1} for –(C=O)); **c** tridimensional view of the FT-IR spectra (in the range 600–4000 cm^{-1}) evolved during GME thermal degradation. The graph shows the temperature range from 120 to 520 °C, highlighting the evolution trend of the main functional groups

composite is bound more strongly compared to GP, likely due to the presence of sugars in the GME extract which can form hydrogen bonds with water molecules, leading to a tighter interaction and higher water retention capacity. It is worth noticing that the FT-IR spectra of the gases evolved during the thermal degradation of GP-GME do not show the presence of residue ethanol (confirming the complete removal of the solvent used during the preparation), nor of CO_2. The latter is often present in many geopolymers formed in an alkaline environment with sodium ions, due to efflorescence phenomena that can occur on the surface [45, 46]. CO_2 absence, therefore, indicates that geopolymerisation has occurred through a stable formulation in which there is a balance of charges due to sodium and aluminium ions [47]. The thermal profiles of the samples show an additional small mass loss (around 2–3% mass loss) between 250 and 900 °C. Even if the identification of the gas evolved in this region by FT-IR spectroscopy was not possible due to the small quantity of gases evolved with respect to the absolute sample mass (a flat FT-IR spectrum was recorded), it is possible to assume, in accordance with the literature, that it was mainly due to the dehydroxylation of the free hydroxyl groups in the aluminosilicate network of the geopolymer, [44] and in case of GP-GME sample, the colourant degradation.

Except for the small differences cited above on the quantity of water entrapped, it can be concluded that the presence of the extract did not alter the thermal stability of the geopolymer.

The geopolymer reticulation stability over time was assessed. Figure 5a shows macroscopic images of the GP and GP-GME samples after 7 and 56 days of ageing times. The picture reveals that the differences between the coloured and non-coloured geopolymers are not fully visible from the outside. However, when split in half, it can be seen that GP is white and has a compact, bubble-free structure, whereas GP-GME is slightly violet/brownish and has some bubbles in the inner part. This colouration seems to remain even after 56 days of ageing. The loss of the strong red colouration of GME, due to the prevalence of the flavilium cation structure of anthocyanins (present at pH below 3, Figure S4), can be attributed to the alkaline environment used for the geopolymerisation reaction. Indeed, GP-GME exhibits a light violet/brownish colouration related to the presence of the quinonoidal and anionic quinonoidal bases of anthocyanins' structures (present at pH 6–7, Figure S5), which can turn to the light-yellow chalcone structure in alkaline environment (above pH 8, Figure S4). This is also in accordance with the CIELab colour space analysis of GP-GME, in which a ΔE value of 4.1 (with respect to GP) was recorded. This value indicates that there is a difference in colour between the two samples, but it is slightly perceptible to the human eye as the value is above 3 and under 5. From a macroscopic point of view, both GP and GP-GME have smooth and homogeneous surfaces, with well-hardened structures. This is also confirmed from a microscopic point of view, since SEM images of GP and GP-GME after 56 days of ageing time (Fig. 5b and c) showed no morphological differences.

Overall, even without the use of purified anthocyanins, the colouration of geopolymers occurred successfully. Nevertheless, it is worth noticing that the use of a synthetic colourant (for example acridine orange) with the same GP formulation induced a better colouration and homogeneous structure (see details in [10]).

The stability of GP and GP-GME over 56 days of ageing time was investigated by measuring the pH and ionic conductivity of a solution of the sample powder in deionised water, as well as by conducting mass loss and integrity tests on samples' pieces.

The measurements of pH and ionic conductivity were recorded over a 72 h period. It is known that large changes in pH and ionic conductivity values of the solution over time are directly linked to an unstable structure. Specifically, they indicate a low degree of networking in the consolidated samples. Indeed, the pH is raised when unbound or unreacted $–OH^-$ groups leak out of the geopolymers, which also contributes to the increase in the conductivity of the leached. This latter is also raised over time when there is an imbalance between positive charges of the Na^+ ions and $[AlO_4]^-$ tetrahedrons in the aged GPs [23, 45, 48].

The trends in pH and ionic conductivity for GP and GP-GME are shown in Figures S6 and S7, respectively. Figure S6a shows that during the ageing time, GP samples have a slight decrease in pH values, which reach a plateau at pH 11.7 at 56 days of ageing only after 6 h of measuring. The absence of a strong increase in pH values over ageing time suggested a stable structure as there was no increment in $–OH^-$ species released. The same pH trend was also present in GP-GME samples, which reached a plateau at pH 12 for all the ageing times without strong variation (Figure S6b).

The study of the network stabilisation followed by the ionic conductivity (Figure S7a) revealed that for GP samples aged 7 days, there was an increase in ionic conductivity with a plateau at 420 mS m^{-1} after 72 h of measurements,

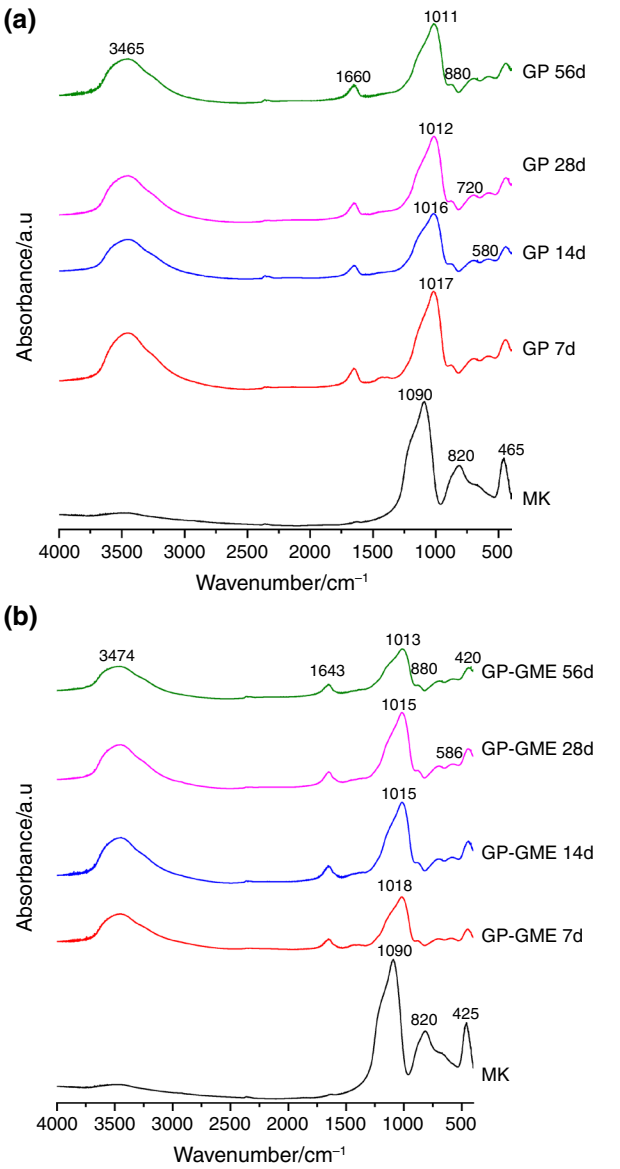

Fig. 3 FT-IR spectra of **a** GP and **b** GP-GME at different ageing times (the letter d stands for days), compared to the MK spectrum

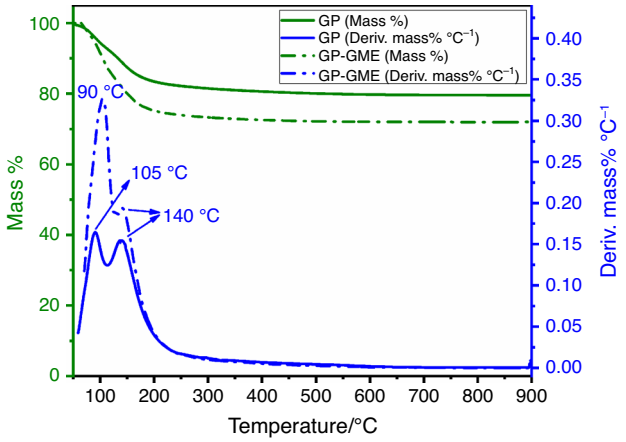

Fig. 4 Curves obtained by TGA of GP and GP-GME. The analysis of the gases evolved during thermal degradation by FT-IR spectroscopy is reported in Fig. S4

whereas, after 14 days of ageing, it reached an ionic conductivity value of 350 mS m^{-1}. The value of the plateau stabilised at 320 mS m^{-1} within 48 h after 28 and 56 days of ageing. Both the information, the time after which the plateau is reached, and the reduction in the conductivity values indicate a decrease in ionic species released in water, thus leading to a more stable structure because the ions are well interconnected in the consolidated structure. In the case of GP-GME (Figure S7b), there was an increase in ionic conductivity plateau up to 14 days (550 mS m^{-1} after 48 h). This phenomenon can be due to the continuous assessment of the 3D network. As the ageing time increases, the conductivity decreases and reaches stable values at 450 mS m^{-1} for both 28 and 56 days, indicating the achievement of structural stability of the ageing geopolymer composite. Furthermore, the higher ionic conductivity values of GP-GME, compared to GP, are probably related to the chalcone leachable in the solution.

The integrity test evaluates the eventual release of substances from the produced geopolymers into the environment, simulating what happens if the material is exposed to the weather [24]. For this purpose, pieces of GP and GP-GME aged 7, 14, 28, and 56 days were soaked in water, observing the integrity of the material in terms of their possible fractures, and the colour and the pH of the leachate after 24 h of testing. The results revealed that the GP sample overcame the integrity test after 28 days of ageing time (no fractures or fragmentations of the sample were detected). On the contrary, GP-GME samples succeeded in the test only after 56 days of ageing time. Moreover, all the leachates of GP-GME samples showed a light-yellow colour with a pH above 9, reinforcing the idea of the partial leaching of chalcone in water.

Regarding the mass loss tests, both samples had a decrease in their mass loss over time (Fig. 6). These decreases in M_L values suggest the progression of geopolymerisation reactions. Indeed, the lower the mass loss, the higher the structure is consolidated. At a molecular level, all the charges are well balanced, and the substitution of silicon atoms with aluminium atoms induces network formation and stability.

Differences in the hardened structures can be also noticed by comparing the mechanical strengths of GP and GP-GME

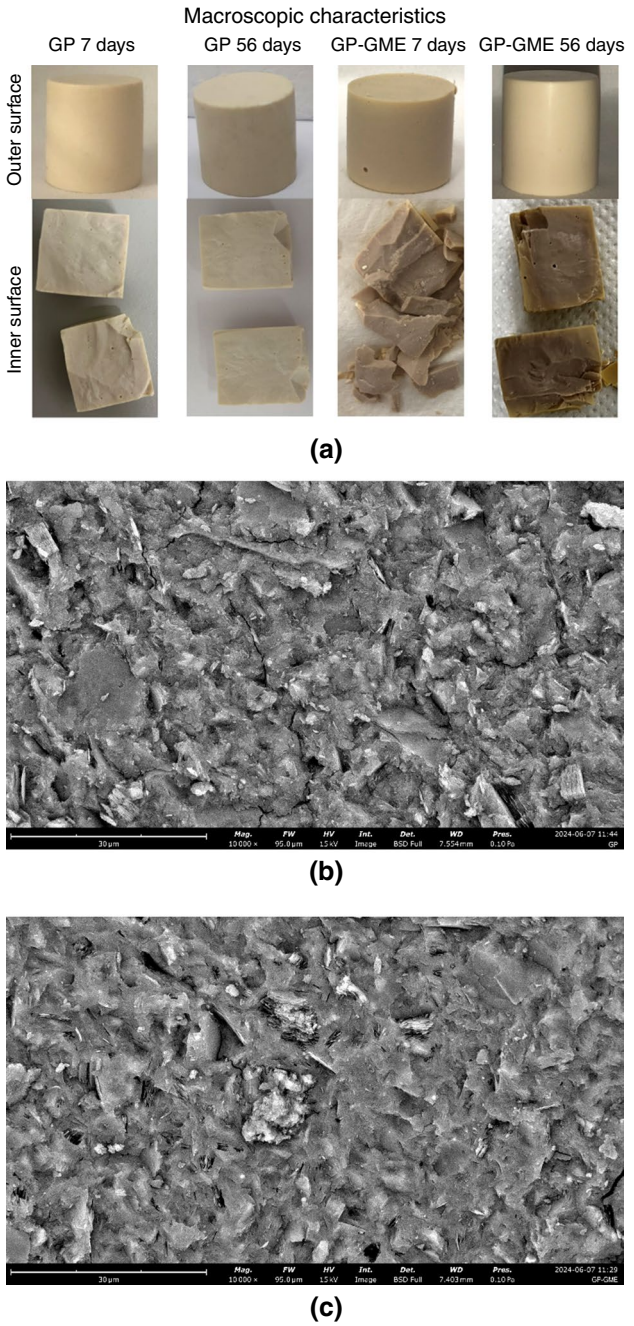

Fig. 5 **a** Comparison of geopolymers after 7 and 56 days of ageing time obtained with and without GME; SEM images of **b** GP and **c** GP-GME

samples after 28 days of ageing time. Indeed, the former showed a compressive strength (22.52 ± 0.22 MPa) higher than the latter obtained in the presence of the grape marc extract (8.46 ± 0.08 MPa). This result can be due to the complexity of the dye extract which has affected the 3D network of the consolidated GP-GME sample. Moreover, in

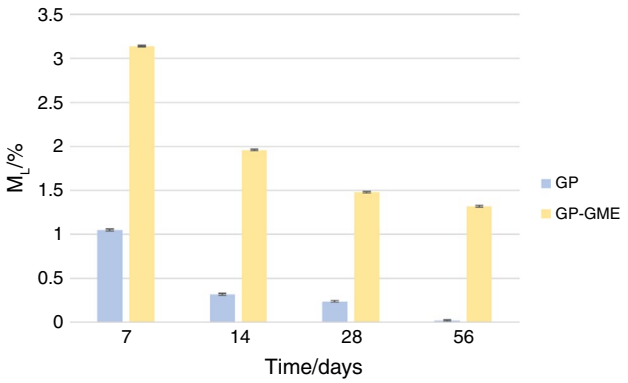

Fig. 6 GP and GP-GME mass loss results at different ageing times

accordance with the literature findings, the higher the ionic conductivity values, the lower the compressive strength [49]. Indeed, GP-GME has higher ionic conductivity values with respect to GP, and this may have a negative impact on the mechanical properties of the former. A suitable strategy to enhance mechanical properties could be the addition of vegetal oil or plant fibres to the fresh geopolymer paste. The former acts as porosity controlling agent and is very useful to get a well-tailored structure thus influencing mechanical strength [50], the latter can be useful to reduce cracks in geopolymer microstructure getting stronger and better mechanical properties [51].

Antimicrobial assessment

The antimicrobial activity of GP and GP-GME (aged at 56 days) against both gram-positive and negative bacteria is reported in Fig. 7.

The images reveal that GM-GME samples have higher antimicrobial activity against *E. coli* (IHD = 1.66 cm and 72.42% of BV) with respect to MK and GP (see also Table S1 in supplementary materials). As regards *S. aureus*, GP-GME showed the same trend as GP and MK. The results are also in accordance with [52] which found that the phenolic compounds from grape extracts possess an increased activity against gram-negative bacteria and a lower effect against gram-positive bacteria. Moreover, the same behaviour can also be observed when phenolic compounds are trapped in inorganic SiO_2 matrices [53]. In contrast, when a synthetic colourant (acridine orange) was used to colour geopolymers, a higher antimicrobial activity was achieved [10]. Nevertheless, it is worth noting that the synthetic colourant can also bind well to human DNA and RNA [54]; therefore, it presents high human toxicity [55]. This problem is instead absent in GP-GME material, which shows good antimicrobial activity without being toxic to human health.

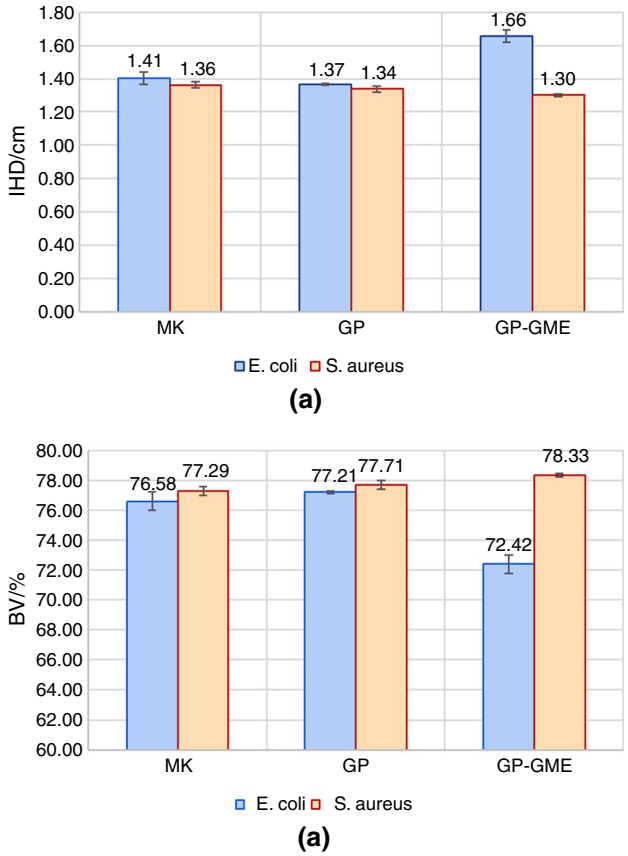

Fig. 7 **a** IHD and **b** Bacterial cell viability values of MK, GP, and GP-GME assayed in the presence of E. coli and S. aureus

Conclusions

Conventional dyeing processes often involve isolating and purifying specific dyeing components, which can be expensive and time-consuming. In this study, a dyeing extract, based on grape marc from an oenological farm, was used as a natural dye to colour a metakaolin-based geopolymer. After its physicochemical characterisation, the extract was added directly to the geopolymer fresh paste without purification of anthocyanins, which simplifies the process and reduces costs. The FT-IR spectroscopic investigation revealed that the presence of GME did not affect the geopolymerisation reactions. Indeed, the red shift of the DOSPM in GP and GP-GME samples revealed the formation of Si–O–Al bonds, thus indicating the effective building of the geopolymer 3D network, as also confirmed by the shift of the main amorphous hump in the XRD pattern. GP-GME was coloured (violet/brownish) with a ΔE of 4.1 with respect to GP, measured by CIElab colour space analysis. This colour comes out from the presence of the quinonoidal and chalcone forms of anthocyanins. Lately, the thermal, mechanical, morphological, and antimicrobial properties of GP-GME were assessed over 56 days of ageing and compared with the blank GP. Thermal analysis showed that GP-GME has the same thermal stability as the white GP control. Besides, the absence of CO_2 gas evolved during thermal analysis in both the samples is straightforward evidence that all the positive sodium ions balanced perfectly with the negative charges coming from aluminium atoms involved in network formation. Therefore, no Na^+ ions on geopolymer surfaces can interact with atmospheric CO_2 causing efflorescence phenomenon. Concerning the other properties studied, all the tests on the geopolymer structure showed that GP-GME reached its structural stability after 56 days of ageing time. Moreover, it possesses an increased activity against *E. coli* but decreased mechanical properties compared to the GP control.

Overall, the material proposed here showed competitive properties with respect to those reported in the literature in which a synthetic dye was used, taking also into account that the GME is non-toxic, recovered by waste biomasses without any further purification of anthocyanins for the sake of sustainability.

The entirety of the properties showed by GP-GME suggests its possible application for covering walls (e.g. hospital or furniture surfaces) or mosaics for restoration, taking advantage of both the antimicrobial and colouration properties given by the presence of the natural dye.

Supplementary Information The online version contains supplementary material available at https://doi.org/10.1007/s10973-024-13482-0.

Acknowledgements The author would like to thank Prochin Italia Prodotti Chimici Industriali Srl (Marcianise, Italy) for the kind donation of the sodium silicate used in this work, Ecoricerche Srl (Capua, Italy) for the SEM images, and Prof Natale Perchiazzi (Department of Earth Science, University of Pisa) for the XRD analyses. The authors want also to thank the PRIN 2022 PNRR project #P2022S4TK2 GLASS-based TREAtments for Sustainable Upcycling of inorganic RESidues for the support on the antimicrobial tests and the University of Pisa (Fondi di Ateneo) for financial support.

Author contributions All authors read and approved the final manuscript. Conceptualisation was done by Antonio D'Angelo and Michelina Catauro; Antonio D'Angelo, Chiara Pelosi, and Elena Pulidori helped in methodology; Antonio D'Angelo, Chiara Pelosi, and Elena Pulidori were involved in formal analysis and investigation; Antonio D'Angelo and Chiara Pelosi contributed to writing—original draft preparation; Michelina Catauro, Maria Rosaria Tiné, and Elena Pulidori contributed to writing—review and editing; Michelina Catauro and Maria Rosaria Tiné helped in funding acquisition; Michelina Catauro assisted in resources; supervision was done by Michelina Catauro and Maria Rosaria Tiné.

Funding Open access funding provided by Università degli Studi della Campania Luigi Vanvitelli within the CRUI-CARE Agreement.

Declarations

Conflict of interest The authors declare no conflict of interest.

References

1. Madia VN, De Vita D, Ialongo D, Tudino V, De Leo A, Scipione L, et al. Recent advances in recovery of lycopene from tomato waste: a potent antioxidant with endless benefits. Molecules. 2021;26:4495.
2. Piccolella, Crescente, Volpe, Paolucci, Pacifico. UHPLC-HR-MS/MS-Guided Recovery of Bioactive Flavonol Compounds from Greco di Tufo Vine Leaves. Molecules [Internet]. 2019, 24:3630
3. Carrillo C, Nieto G, Martínez-Zamora L, Ros G, Kamiloglu S, Munekata PES, et al. Novel approaches for the recovery of natural pigments with potential health effects. J Agric Food Chem. 2022;70(6864–83):8.
4. Szabo K, Teleky B-E, Ranga F, Roman I, Khaoula H, Boudaya E, et al. Carotenoid recovery from tomato processing by-products through green chemistry. Molecules. 2022;27:3771.
5. ISTAT Cultivation: Grape, Wine, Olive, Oil [Internet]. [cited 2024 Feb 1]
6. Zacharof M-P. Grape winery waste as feedstock for bioconversions: applying the biorefinery concept. Waste Biomass Valoriz. 2017;8:1011–25.
7. Davidovits J. Geopolymers: ceramic-like inorganic polymers. J Ceram Sci Technol. 2017;8:335–50.
8. Davidovits J. Geopolymer: chemistry & applications. 5th editio. Institut Géopolymère: Saint-Quentin. 2020
9. Ouellet-Plamondon C, Aranda P, Favier A, Habert G, van Damme H, Ruiz-Hitzky E. The Maya blue nanostructured material concept applied to colouring geopolymers. RSC Adv. 2015;5:98834–41.
10. D'Angelo A, Vertuccio L, Leonelli C, Alzeer MIM, Catauro M. Entrapment of acridine orange in metakaolin-based geopolymer: a feasibility study. Polymers (Basel). 2023;15:675.
11. D'Angelo A, Dal Poggetto G, Piccolella S, Leonelli C, Catauro M. Characterisation of white metakaolin-based geopolymers doped with synthetic organic dyes. Polymers (Basel). 2022;14:3380.
12. Neto JSS, de Queiroz HFM, Aguiar RAA, Banea MD. A Review on the thermal characterisation of natural and hybrid fiber composites. Polymers (Basel). 2021;13:4425.
13. Pulidori E, Micalizzi S, Bramanti E, Bernazzani L, De Maria C, Pelosi C, et al. Valorization of not soluble byproducts deriving from green keratin extraction from poultry feathers as filler for biocomposites. J Therm Anal Calorim. 2022. https://doi.org/10.1007/s10973-021-11166-7.
14. Ghetti P, Ricca L, Angelini L. Thermal analysis of biomass and corresponding pyrolysis products. Fuel. 1996;75:565–73.
15. Pulidori E, Gonzalez-rivera J, Pelosi C, Ferrari C, Bernazzani L, Bramanti E, et al. Thermochemical evaluation of different waste biomasses (citrus peels, aromatic herbs, and poultry feathers) towards their use for energy production. Thermo. 2023;3(1):66–75.
16. Menczel JD, Prime RB. Thermal Analysis of Polymers [Internet]. Menczel JD, Prime RB, editors. Wiley; 2009
17. Gałko G, Sajdak M. Trends for the thermal degradation of polymeric materials: analysis of available techniques, issues, and opportunities. Appl Sci. 2022;12:9138.
18. Gonzalez-Rivera J, Pelosi C, Pulidori E, Duce C, Tiné MR, Ciancaleoni G, et al. Guidelines for a correct evaluation of deep eutectic solvents thermal stability. Curr Res Green Sustain Chem. 2022, 100333
19. Ramachandran V, Paroli R, Beaudoin J. Handbook of Thermal Analysis of Construction Materials. 2002
20. Kaze CR, Nana A, Lecomte-Nana GL, Deutou JGN, Kamseu E, Melo UC, et al. Thermal behaviour and microstructural evolution of metakaolin and meta-halloysite-based geopolymer binders: a comparative study. J Therm Anal Calorim. 2022;147:2055–71.
21. Cao VD, Pilehvar S, Salas-Bringas C, Szczotok AM, Bui TQ, Carmona M, et al. Thermal analysis of geopolymer concrete walls containing microencapsulated phase change materials for building applications. Sol Energy. 2019;178:295–307.
22. Nath SK, Mukherjee S, Maitra S, Kumar S. Kinetics study of geopolymerization of fly ash using isothermal conduction calorimetry. J Therm Anal Calorim. 2017;127:1953–61. https://doi.org/10.1007/s10973-016-5823-x.
23. Sgarlata C, Formia A, Ferrari F, Leonelli C. Effect of the Introduction of reactive fillers and metakaolin in waste clay-based materials for geopolymerization Processes. Molecules. 2021;26:1325.
24. Zuaiter M, El-Hassan H, El-Maaddawy T, El-Ariss B. Properties of slag-fly ash blended geopolymer concrete reinforced with hybrid glass fibers. Buildings. 2022;12:1114.
25. EUROPEAN STANDARDS DIN EN 826- Thermal Insulating Products for Building Applications - Determination of Compression Behaviour.
26. Velho SRK, Brum LFW, Petter CO, dos Santos JHZ, Šimunić Š, Kappa WH. Development of structured natural dyes for use into plastics. Dye Pigment. 2017;136:248–54.
27. Hudzicki J, Disk K-B. Diffusion Susceptibility Test Protocol. 2009
28. Anjos O, Santos AJA, Estevinho LM, Caldeira I. FTIR–ATR spectroscopy applied to quality control of grape-derived spirits. Food Chem. 2016;205:28–35.
29. Casazza AA, Aliakbarian B, Lagazzo A, Garbarino G, Carnasciali MM, Perego P, et al. Pyrolysis of grape marc before and after the recovery of polyphenol fraction. Fuel Process Technol. 2016;153:121–8.
30. Farru G, Cappai G, Carucci A, De Gioannis G, Asunis F, Milia S, et al. A cascade biorefinery for grape marc: recovery of materials and energy through thermochemical and biochemical processes. Sci Total Environ. 2022;846:157464.
31. Garrido T, Gizdavic-Nikolaidis M, Leceta I, Urdanpilleta M, Guerrero P, de la Caba K, et al. Optimizing the extraction process of natural antioxidants from chardonnay grape marc using microwave-assisted extraction. Waste Manag. 2019;88:110–7.
32. Olejar KJ, Ricci A, Swift S, Zujovic Z, Gordon KC, Fedrizzi B, et al. Characterization of an antioxidant and antimicrobial extract from cool climate, white grape marc. Antioxidants. 2019;8:232.
33. Silverstein RM, Webster FX, Kiemle DJ, Bryce DL. Spectrometric identification of organic compounds. 8th ed. New Jersey: Wiley; 2014.
34. Torres-Garcia E, Brachi P. Non-isothermal pyrolysis of grape marc: thermal behavior, kinetics and evolved gas analysis. J Therm Anal Calorim. 2020;139:1463–78. https://doi.org/10.1007/s10973-019-08530-z.
35. Khiari B, Jeguirim M. Pyrolysis of grape marc from Tunisian wine industry: Feedstock characterization, thermal degradation and kinetic analysis. Energies. 2018;11(4):730. https://doi.org/10.3390/en11040730.

36. Varol EA, Mutlu Ü. TGA-FTIR analysis of biomass samples based on the thermal decomposition behavior of hemicellulose, cellulose, and lignin. Energies. 2023;16(9):3674. https://doi.org/10.3390/en16093674.
37. Djobo JNY, Tchadjié LN, Tchakoute HK, Kenne BBD, Elimbi A, Njopwouo D. Synthesis of geopolymer composites from a mixture of volcanic scoria and metakaolin. J Asian Ceram Soc. 2014;2:387–98.
38. Sitarz M, Handke M, Mozgawa W. Identification of silicooxygen rings in SiO_2 based on IR spectra. Spectrochim Acta Part A Mol Biomol Spectrosc. 2000;56:1819–23.
39. Catauro M, Dal Poggetto G, Sgarlata C, Vecchio Ciprioti S, Pacifico S, Leonelli C. Thermal and microbiological performance of metakaolin-based geopolymers cement with waste glass. Appl Clay Sci. 2020;197:105763.
40. Kamseu E, Alzari V, Nuvoli D, Sanna D, Lancellotti I, Mariani A, et al. Dependence of the geopolymerization process and end-products to the nature of solid precursors: challenge of the sustainability. J Clean Prod. 2021;278:123587.
41. Nmiri A, Duc M, Hamdi N, Yazoghli-Marzouk O, Srasra E. Replacement of alkali silicate solution with silica fume in metakaolin-based geopolymers. Int J Miner Metall Mater. 2019;26:555–64.
42. Chen L, Wang Z, Wang Y, Feng J. Preparation and properties of alkali activated metakaolin-based geopolymer. Materials. 2016;9(9):767. https://doi.org/10.3390/ma9090767.
43. Pelosi C, Occhipinti R, Finocchiaro C, Lanzafame G, Pulidori E, Lezzerini M, et al. Thermal and morphological investigations of alkali activated materials based on Sicilian volcanic precursors (Italy). Mater Lett. 2023;335:133773. https://doi.org/10.1016/j.matlet.2022.133773.
44. Pulidori E, Lluveras-Tenorio A, Carosi R, Bernazzani L, Duce C, Pagnotta S, et al. Building geopolymers for CuHe part I: thermal properties of raw materials as precursors for geopolymers. J Therm Anal Calorim. 2022;147:5323–35.
45. Liang K, Cui K, Sabri MMS, Huang J. Influence factors in the wide application of alkali-activated materials: a critical review about efflorescence. Materials. 2022;15(18):6436. https://doi.org/10.3390/ma15186436.
46. Catauro M, Viola V, D'Amore A. Mosses on geopolymers: preliminary durability study and chemical characterization of metakaolin-based geopolymers filled with wood ash. Polymers. 2023;15(7):1639. https://doi.org/10.3390/polym15071639.
47. Simão L, Fernandes E, Hotza D, Ribeiro MJ, Montedo ORK, Raupp-Pereira F. Controlling efflorescence in geopolymers: a new approach. Case Stud Constr Mater. 2021;15:e00740.
48. Sá Ribeiro RA, Sá Ribeiro MG, Kutyla GP, Kriven WM. Amazonian metakaolin reactivity for geopolymer synthesis. Adv Mater Sci Eng. 2019;2019:1–7.
49. Dal Poggetto G, D'Angelo A, Catauro M, Barbieri L, Leonelli C. Recycling of waste corundum abrasive powder in MK-based geopolymers. Polymers. 2022;14(11):2173. https://doi.org/10.3390/polym14112173.
50. Seyrek Y, Rudic O, Mittermayr F, Grengg C, Freytag B, Juhart J. Impact of humidity and vegetable oil addition on mechanical properties and porosity of geopolymers. Cem Concr Compos. 2023;140:105083.
51. Lv C, Wu D, Guo G, Zhang Y, Liu S, Qu E, et al. Effect of plant fiber on early properties of geopolymer. Molecules. 2023;28:4710.
52. Cueva C, Mingo S, Muñoz-González I, Bustos I, Requena T, del Campo R, et al. Antibacterial activity of wine phenolic compounds and oenological extracts against potential respiratory pathogens. Lett Appl Microbiol. 2012;54:557–63.
53. Petrelli V, Dell'Anna MM, Mastrorilli P, Viola V, Catauro M, D'Angelo A. Synthesis by sol-gel route of organic-inorganic hybrid material: chemical characterization and in vitro release study. Appl Sci. 2023;13:8410.
54. Yektaeian N, Mehrabani D, Sepaskhah M, Zare S, Jamhiri I, Hatam G. Lipophilic tracer Dil and fluorescence labeling of acridine orange used for Leishmania major tracing in the fibroblast cells. Heliyon. 2019;5:e03073.
55. Valentini A, Pucci D, Crispini A, Federici G, Bernardini S. Acridine orange based platinum(II) complexes inducing cytotoxicity and cell cycle perturbation in spite of GSTP1 up-regulation. Chem Biol Interact. 2006;161:241–50.

Authors and Affiliations

Chiara Pelosi[1] · Elena Pulidori[1] · Antonio D'Angelo[2] · Maria Rosaria Tiné[1] · Michelina Catauro[2]

✉ Antonio D'Angelo
antonio.dangelo@unicampania.it

[1] Department of Chemistry and Industrial Chemistry, University of Pisa, Via G. Moruzzi 13, 56124 Pisa, Italy

[2] Department of Engineering, University of Campania ''Luigi Vanvitelli'', Via Roma 29, 81031 Aversa, Italy